Spatial and temporal distribution of *Q*-switched laser pulses in multimode regimes

Ming Yin (阴 明)[1], Guoying Feng (冯国英)[1*], Shutong Wang (王树同)[1], Huomu Yang (杨火木)[1], and Shouhuan Zhou (周寿桓)[1,2]

[1] *College of Electronics and Information Engineering, Sichuan University, Chengdu 610065, China*

[2] *North China Research Institute of Electro-Optics, Beijing100015, China*

[*] *Corresponding author: guoing_feng@scu.edu.cn*

Received September 26, 2013; accepted November 5, 2013; posted online December 9, 2013

The spatial and temporal distribution of *Q*-switched diode-pumped solid-state laser (DPSSL) pulses is investigated in multimode regimes. A theory model of spatial and temporal distribution of multimode *Q*-switched DPSSL pulses is established. The influences of position, initial population inversion density, and mode ratio on pulse width are studied. The results show that the pulse expands in the position wherein two or more mode intensities are equivalent, and the pulse building time difference of the modes are less than one mode pulse width. These results can be applied in pulse compression and mode composition.

OCIS codes: 140.0140, 140.3480, 140.3538.

doi: 10.3788/COL201311.121405.

Q-switched diode-pumped solid-state lasers (DPSSLs) are a hot topic in research[1−4] because of their wide variety of applications, such as material processing, nonlinear optics, remote sensing, medical applications, and laser ranging[5−8]. Much attention has been paid to pulse width research[9−11] because most existing applications depend on the operation pulse width[12−14]. The pulse width of *Q*-switched lasers is calculated under a top-hat pump beam distribution[9]. The pulse width of miniature passively *Q*-switched lasers are calculated accounting for thermalization and relaxation processes[10]. The pulse shape of *Q*-switched lasers has been described in detail in multimode regimes[11]. However, research on the spatial and temporal distribution of *Q*-switched DPSSL pulses has not been reported. The spatial distribution of pulse width in *Q*-switched DPSSLs in a single mode has been studied recently[15,16]. For multimode lasers, the spatial and temporal distribution of *Q*-switched DPSSL pulses should be investigated in multimode regimes.

In this letter, an acousto-optic (AO) *Q*-switched DPSSL is built. The spatial and temporal distribution of multimode *Q*-switched DPSSL pulses is measured. A theory model of the spatial and temporal distribution of multimode *Q*-switched DPSSL pulses is established. The influences of position, initial population inversion density, and mode ratio on pulse width are investigated in multimode regimes. The pulse expands in the position wherein two or more mode intensities are equivalent and the pulse building time difference of the modes is less than one mode pulse width. These results can be used in pulse compression and mode composition in *Q*-switched DPSSLs.

The experimental setup is shown in Fig. 1. The resonator is formed by two plane mirrors (M_1 and M_2). Plane mirror M_1 is coated for high reflection at 1064 nm. The output coupler M_2 is a plane mirror with 10% transmission at 1064 nm. The optical pump source consists of three laser-diode bars. The pump lights are placed in the laser rod from three symmetrical directions. The laser medium is 0.6 at.-% Nd-doped Nd:YAG crystal with dimensions of $\phi 4\times 65$ (mm). This crystal is coated for antireflection at 1064 nm on its two end faces to decrease the loss of the laser cavity. The crystal is then cooled by flowing water at a temperature of 20 °C. The AO *Q*-switch with high diffraction loss at 1064 nm is placed inside the cavity, and its repetition rate is tuned continuously from 0.5 to 50 kHz. In this letter, we choose 3 kHz for the experiment. The cavity length is 250 mm. The temporal shape of the output laser pulse is recorded by a photodiode detector (rise time of less than 15 ns) with a small hole fixed on the motorized stage and a fast digital oscilloscope (Tektronix DPO4032, 350-MHz bandwidth, 3.5-GS/s sampling rate). The laser reflected by an optical wedge is measured to protect the detector.

The intensity distributions of a laser beam with pump currents of 12 and 13 A are shown in Figs. 2(a) and (b), respectively. The position value represents the distance between the center of the beam cross section and the measurement position. The experimental intensity values are fitted by the Gaussian function. The beam radii with pump currents of 12 and 13 A are 1.309 and 1.556 mm, respectively. The fundamental mode radii with pump currents of 12 and 13 A are calculated to be 0.923 and

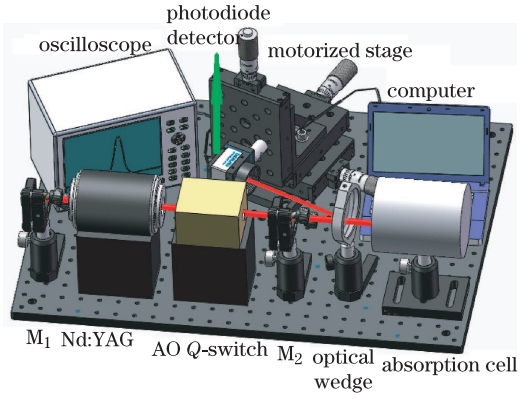

Fig. 1. Schematic of the experimental setup.

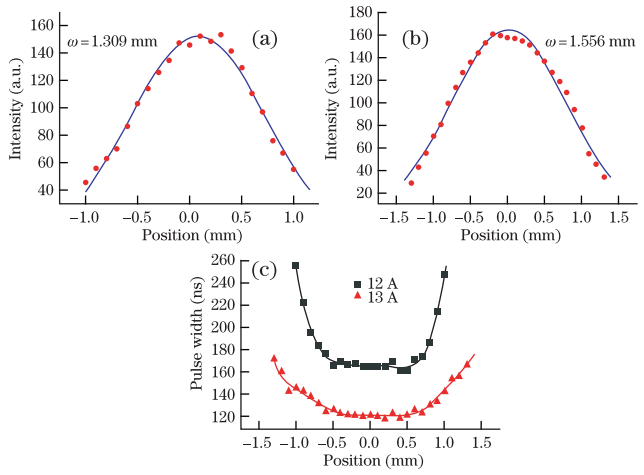

Fig. 2. Intensity distributions of a laser beam with pump currents of (a) 12 A and (b) 13 A; (c) Pulse width as a function of position within the beam cross section for different pump currents.

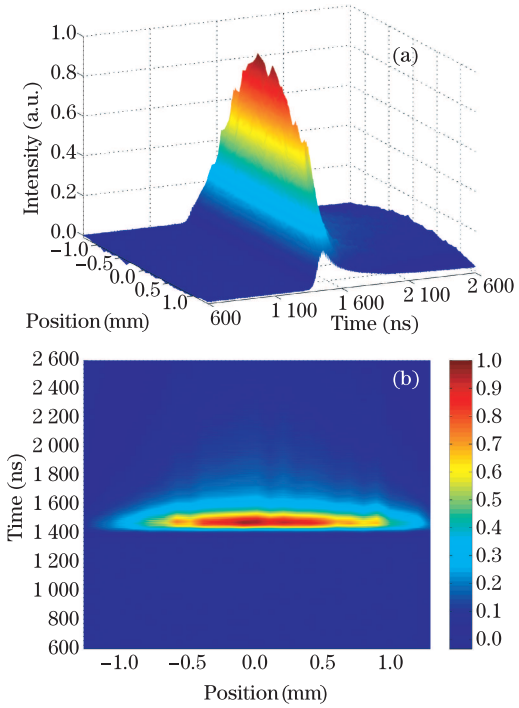

Fig. 3. (a) Spatial and temporal distribution of the Q-switched DPSSL pulse shown in Fig. 2(b); (b) Top view of the distribution.

0.963 mm, respectively, accounting for the thermal focal length of the laser rod. Thus, the laser operates in multimode regimes. Figure 2(c) shows the variation of the pulse width as a function of position within the beam cross section for different pump currents. The pulse width increases with increasing position for a given pump current. The influence of position on pulse width is relatively small in the center of the beam cross section and relatively large at the edge of the beam cross section. The case of 12 A is taken as an example. When the position increases from 0 to 0.7 mm, the increment of the pulse width is only 7.9 ns. When the position increases from 0.7 to 1.0 mm, the increment of the pulse width is 63.9 ns. As shown in Fig. 2(c), when the pump current is small, the pulse width is large.

Figure 3 presents the spatial and temporal distribution of the Q-switched DPSSL pulse shown in Fig. 2(b). Based on Fig. 3, the distribution is asymmetrical in the temporal domain and symmetrical in the spatial domain.

The rate equations with the spatial distribution of population inversion density and photon density are given as[17]

$$\int_a \frac{\mathrm{d}\phi(r,\theta,t)}{\mathrm{d}t}\mathrm{d}V = \int_a \left[\phi(r,\theta,t)c\sigma n(r,\theta,t)\frac{l'}{L} - \frac{\phi(r,\theta,t)\xi}{t_r}\right]\mathrm{d}V, \quad (1)$$

$$\frac{\mathrm{d}n(r,\theta,t)}{\mathrm{d}t} = G(r,\theta) - \frac{n(r,\theta,t)}{t_f} - \gamma n(r,\theta,t)\phi(r,\theta,t)\sigma c, \quad (2)$$

where $\phi(r,\theta,t)$ is the photon density, $n(r,\theta,t)$ is the population inversion density, $G(r,\theta)$ is the pumping rate per unit volume, c is the speed of light in vacuum, σ is the stimulated emission cross section, l' is the length of the active material, L is the optical length of the resonator, ξ is the loss per round trip, t_r is the round-trip time, γ is the inversion reduction factor, and t_f is the upper state lifetime. In Eq. (1), the integral is calculated over the entire volume of the cavity. The loss per round trip can be represented as

$$\xi = -\ln R + \delta, \quad (3)$$

where the first term represents the output coupling losses determined by mirror reflectivity R, and δ contains all incidental losses such as scattering, diffraction, and absorption.

In all cases of interest, the Q-switched pulse duration is extremely short, such that we can neglect spontaneous emission and optical pumping in writing Eq. (2). Hence,

$$\frac{\mathrm{d}n(r,\theta,t)}{\mathrm{d}t} = -\gamma n(r,\theta,t)\phi(r,\theta,t)\sigma c. \quad (4)$$

In a multimode case, the rate equations can be written from Eqs. (1) and (4) as

$$\int_a \frac{\mathrm{d}\phi_\mathrm{pl}(r,\theta,t)}{\mathrm{d}t}\mathrm{d}V = \int_a \left[\phi_{pl}(r,\theta,t)c\sigma n(r,\theta,t)\frac{l'}{L} - \frac{\phi_\mathrm{pl}(r,\theta,t)\xi}{t_r}\right]\mathrm{d}V, \quad (5)$$

$$\frac{\mathrm{d}n(r,\theta,t)}{\mathrm{d}t} = -\gamma n(r,\theta,t)\sum_{p=0}^{p}\sum_{l=0}^{l}\phi_\mathrm{pl}(r,\theta,t)\sigma c, \quad (6)$$

where $\phi_\mathrm{pl}(r,\theta,t)$ is the photon density of the $\mathrm{TEM_{pl}}$ mode. The integers p and l represent the number of nodes with zero intensity that are transverse to the beam axis in radial and angular directions.

In cylindrical coordinates, the photon density spatial distribution of different modes is given by[18]

$$\phi_\mathrm{pl}(r,\theta) = \rho^l[L_\mathrm{p}^l(\rho)]^2\cos^2(l\theta)\exp(-\rho), \quad (7)$$

with $\rho = 2r^2/\omega_0^2$, where r and θ are the polar coordinates in a plane that is transverse to the beam direction, and

Table 1. Parameter Values Used in the Calculation[18]

Parameter	Value	Parameter	Value
c	3×10^8 m/s	δ_{00}	0.0092
σ	2.8×10^{-19} cm^2	δ_{01}	0.0482
l	0.065 m	δ_{10}	0.0232
L	0.25 m	δ_{02}	0.0593
R	90%	δ_{20}	0.0418
t_r	2.022×10^{-9} s		
γ	1		

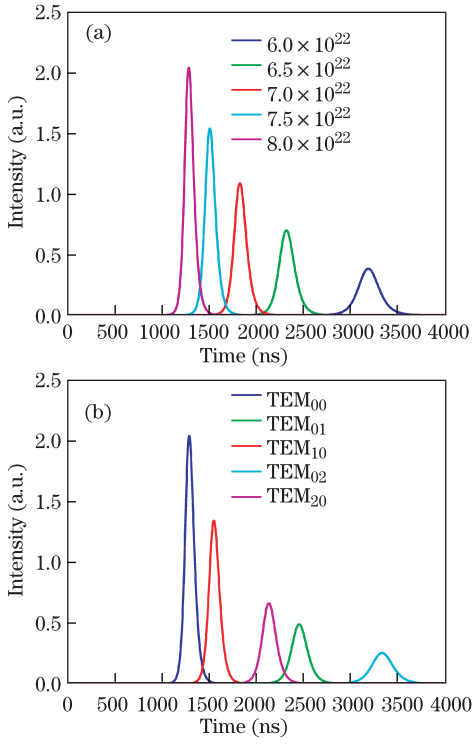

Fig. 4. (a) Pulse shape of the fundamental mode for different initial population inversion densities n_0; (b) Pulse shape of different modes for the initial population inversion density $n_0 = 8.0 \times 10^{22}$.

L_p^l is the generalized Laguerre polynomial of order p and index l.

Based on Eqs. (3), (5), and (6), the pulse shape of the fundamental mode can be calculated simply for different initial population inversion densities n_0, as shown in Fig. 4(a). Different modes correspond to different δvalues, and the pulse shape of different modes can be calculated for the same initial population inversion density n_0, as shown in Fig. 4(b). The parameter values used in the calculation are shown in Table 1. δ_{pl} is the loss per round trip of the TEM_{pl} mode.

As shown in Fig. 4, pulse building time and pulse width decrease with increasing initial population inversion density for a single mode. For different modes, the oscillation threshold of the lower loss mode is smaller than that of the higher loss mode. Hence, the pulse building time of the lower loss mode is shorter than that of the higher loss mode for the same initial population inversion density. The pulse width is mainly determined by the ratio of the initial population inversion density to the threshold. The threshold of the lower loss mode is smaller than that of the higher loss mode, and the ratio of the initial population inversion density to the threshold of the lower loss mode is larger than that of the higher loss mode for the same initial population inversion density. Thus, the pulse width of the lower loss mode is smaller than that of the higher loss mode. The loss of the fundamental mode is smaller than that of the higher-order modes, and thus, the pulse building time of the fundamental mode is shorter than those of the higher-order modes. The pulse width of the fundamental mode is also smaller than those of the higher-order modes for the same initial population inversion density.

Figure 5 shows the spatial and temporal distribution of the Q-switched DPSSL pulse in the fundamental mode for the initial population inversion density $n_0 = 0.8 \times 10^{23}$.

Figure 6 shows the spatial and temporal distribution of the Q-switched DPSSL pulse in multimode regimes for the initial population inversion density $n_0 = 1.695 \times 10^{23}$ and the mode ratio TEM_{00}:TEM_{01}= 55:45.

As shown in Figs. 5 and 6, the intensities of the TEM_{00} and the TEM_{01} modes are equivalent at the edge of the beam, and the pulse building times of the two modes are different. Hence, the pulse at the edge of the beam cross section is "thicker" than that in the center.

Figure 7 shows the variation of the pulse width as a function of the position within the beam cross section for different initial population inversion densities n_0 and mode ratios TEM_{00}:TEM_{01}. The pulse width does not change with increasing position in the fundamental mode, as predicted in Ref. [16], whereas it changes with increasing position for a given initial population inversion

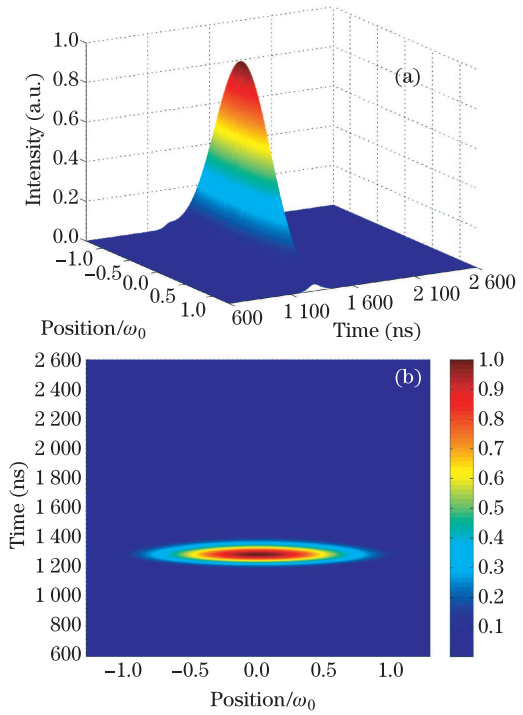

Fig. 5. (a) Spatial and temporal distribution of the Q-switched DPSSL pulse in the fundamental mode for the initial population inversion density $n_0 = 0.8 \times 10^{23}$; (b) Top view of the distribution.

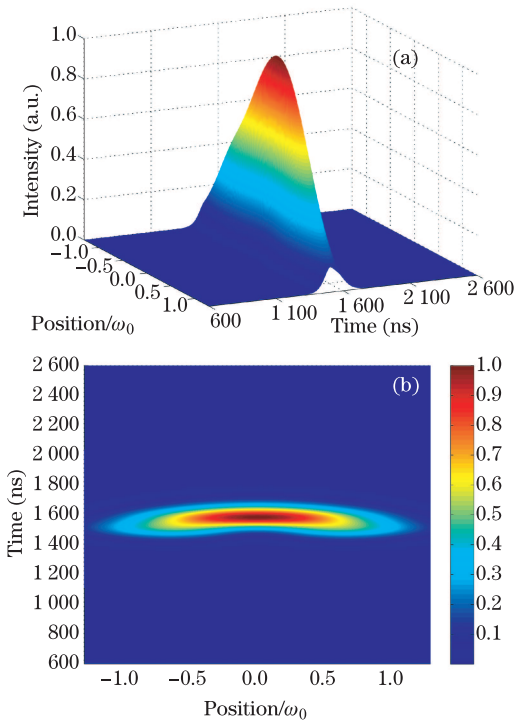

Fig. 6. (a) Spatial and temporal distribution of the Q-switched DPSSL pulse in multimode regimes for the initial population inversion density $n_0 = 1.695 \times 10^{23}$ and the mode ratio $\mathrm{TEM_{00}}$:$\mathrm{TEM_{01}}$= 55:45; (b) Top view of the distribution.

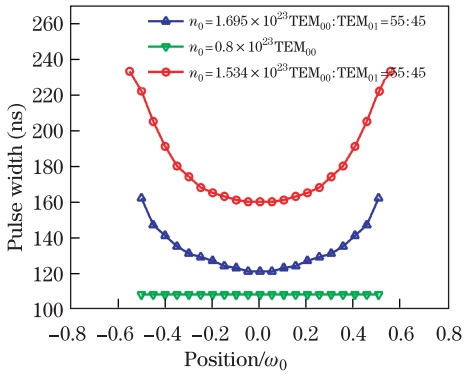

Fig. 7. Pulse width as a function of the position within the beam cross section for different initial population inversion densities n_0 and mode ratios $\mathrm{TEM_{00}}$:$\mathrm{TEM_{01}}$.

density n_0 in multimode regimes. The pulse building times of the $\mathrm{TEM_{00}}$ and the $\mathrm{TEM_{01}}$ modes are different, and thus, the pulse is the superposition of these modes. The intensities of the $\mathrm{TEM_{00}}$ and the $\mathrm{TEM_{01}}$ modes are equivalent at the edge of the beam. Thus, the total pulse width at the edge of the beam cross section is equal to the sum of the $\mathrm{TEM_{00}}$ pulse width and the $\mathrm{TEM_{01}}$ pulse width, minus the superposition width of the two modes.

Figure 8 shows the variation of pulse width as a function of the position within the beam cross section for different initial population inversion densities n_0 and the mode ratio $\mathrm{TEM_{00}}$:$\mathrm{TEM_{01}}$= 55.5:44.5. Pulse width increases with increasing position for a given initial population inversion density n_0. The influence of position on pulse width is relatively small in the center area of the beam cross section and relatively large at the edge of the beam cross section. The pulse width difference between the center and the edge of the beam cross section initially increases and then decreases with increasing initial population inversion density n_0 for a given mode ratio $\mathrm{TEM_{00}}$:$\mathrm{TEM_{01}}$. The pulse building time differences between the $\mathrm{TEM_{00}}$ and the $\mathrm{TEM_{01}}$ modes are 67, 102, 79, 57, and 45 ns for $n_0 = 1.4 \times 10^{23}$, 1.5×10^{23}, 1.6×10^{23}, 1.7×10^{23}, and 1.8×10^{23}, respectively. When the pulse building time difference between the $\mathrm{TEM_{00}}$ and the $\mathrm{TEM_{01}}$ modes is large, then the pulse width difference between the center and the edge of the beam cross section is also large. Therefore, the pulse width difference between the center and the edge of the beam cross section, and the pulse building time difference between the $\mathrm{TEM_{00}}$ and the $\mathrm{TEM_{01}}$ modes exhibit the same trend.

Figure 9 shows the variation of pulse width as a function of the position within the beam cross section for different mode ratios of $\mathrm{TEM_{00}}$ and $\mathrm{TEM_{01}}$ and the initial population inversion density $n_0 = 1.534 \times 10^{23}$. The pulse width difference between the center and the edge of the beam cross section initially decreases and then increases with the increasing mode ratio of $\mathrm{TEM_{00}}$ and $\mathrm{TEM_{01}}$ for a given initial population inversion density n_0. This scenario is caused by the pulse building time of the $\mathrm{TEM_{01}}$ mode being initially shorter than, then the same as, and finally, lasting longer than the pulse building time of the $\mathrm{TEM_{00}}$ mode with the increasing mode ratio of $\mathrm{TEM_{00}}$ and $\mathrm{TEM_{01}}$ for a given initial population inversion density n_0.

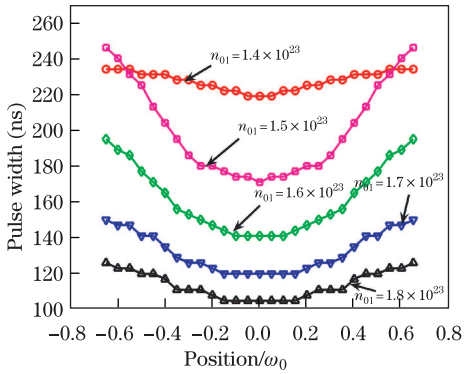

Fig. 8. Pulse width as a function of the position within the beam cross section for different initial population inversion densities n_0 and the mode ratio $\mathrm{TEM_{00}}$:$\mathrm{TEM_{01}}$= 55.5:44.5.

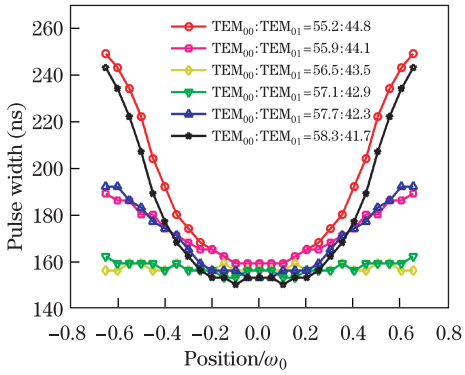

Fig. 9. Pulse width as a function of the position within the beam cross section for different mode ratios of $\mathrm{TEM_{00}}$ and $\mathrm{TEM_{01}}$ and the initial inversion population density $n_0 = 1.534 \times 10^{23}$.

In conclusion, the spatial and temporal distribution of Q-switched DPSSL pulses is investigated experimentally and theoretically in multimode regimes. The results show that pulse width does not change with increasing position in a single mode, but changes with increasing position for a given initial population inversion density n_0 in multimode regimes. The pulse width difference between the center and the edge of the beam cross section initially increases and then decreases with increasing initial population inversion density for a given mode ratio. The pulse width difference between the center and the edge of the beam cross section initially decreases and then increases with increasing fundamental mode ratio for a given initial population inversion density. The pulse expands in the position wherein two or more modes intensities are equivalent and the pulse building time difference of the modes are less than one mode pulse width. The results of this study can be used in pulse compression and mode composition in Q-switched DPSSLs.

This work was supported by the Major Program of the National Natural Science Foundation of China under Grant No. 60890200.

References

1. J. Yu, B. Trieu, E. Modlin, U. Singh, M. Kavaya, S. Chen, Y. Bai, P. Petzar, and M. Petros, Opt. Lett. **31,** 462 (2006).
2. K. Du, D. Li, H. Zhang, P. Shi, X. Wei, and R. Diart, Opt. Lett. **28,** 87 (2003).
3. S. Shu, T. Yu, R. Liu, J. Hou, X. Hou, and W. Chen, Chin. Opt. Lett. **9,** 091407 (2011).
4. T. Lu, J. Wang, M. Huang, D. Liu, and X. Zhu, Chin. Opt. Lett. **10,** 081403 (2012).
5. T. Lu, J. Wang, M. Huang, D. Liu, and X. Zhu, Chinese J. Lasers (in Chinese) **39,** 0902002 (2012).
6. P. He, H. Wang, L. Zhang, J. Wang, C. Mo, C. Wang, and X. Li, Opt. Laser Technol. **44,** 631 (2012).
7. A. Zajac, M. Skorczakowski, J. Swiderski, and P. Nyga, Opt. Express **12,** 5125 (2004).
8. Y. Wang, X. Duan, L.Ke, B.Yao, and G. Zhao, Chinese J. Lasers (in Chinese) **36,** 1710 (2009).
9. S. Li, X. Zhang, Q. Wang, P. Li, J. Chang, X. Zhang, and Z. Cong, Appl. Phys. B **88,** 221 (2007).
10. E. Raikkonen, S. Buchter, and M. Kaivola, IEEE J. Quantum Electron. **45,** 1563 (2009).
11. M. Wohlmuth, C. Pflaum, K. Altmann, M. Paster, and C.Hahn, Opt. Express **17,** 17303 (2009).
12. S. Cho, Y. Kim, J. Heo, and J. Lee, Opt. Express **13,** 9472 (2005).
13. K. Shinkawa, and K. Ogusu, Opt. Express **16,** 18230 (2008).
14. F. Wang, X. Wang, X. Zhang, M. Chen, and Y. Lu, Appl. Opt. **51,** 8498 (2012).
15. C. Zhang, X. Zhang, Q. Wang, Z. Cong, and H. Xu, IEEE J. Quantum Electron. **47,** 455 (2011).
16. X. Zhang, S. Zhao, Q. Wang, B. Ozygus, and H. Weber, IEEE J. Quantum Electron. **35,** 1912 (1999).
17. P. Laporta, and M. Brussard, IEEE J. Quantum Electron. **27,** 2319 (1991).
18. W. Koechner, *Solid-State Laser Engineering* (Springer, New York, 2006).